Article

Cell Reports

Flt3L-Mediated Expansion of Plasmacytoid Dendritic Cells Suppresses HIV Infection in Humanized Mice

Graphical Abstract

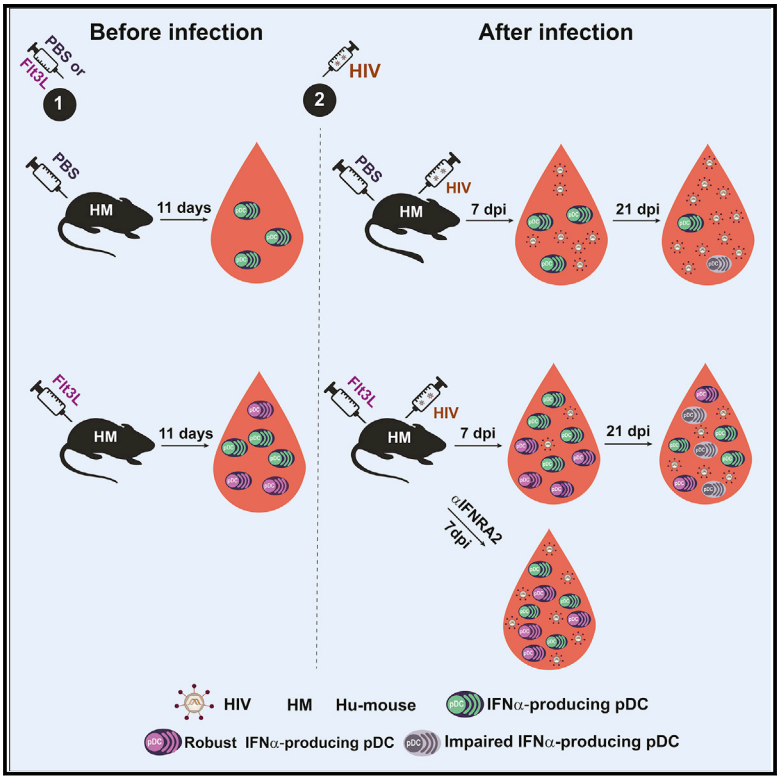

Authors

Tram N.Q. Pham, Oussama Meziane, Mohammad Alam Miah, ..., Cheolho Cheong, Élie Haddad, Éric A. Cohen

Correspondence

tram.pham@ircm.qc.ca (T.N.Q.P.), eric.cohen@ircm.qc.ca (É.A.C.)

In Brief

Plasmacytoid DC (pDC) are vital for a host's early antiviral responses. Pham et al. demonstrate that HIV infection of hu-mice induces widespread depletion of pDC and impairs their ability to make IFN-α. Flt3L treatment expands pDC and suppresses HIV replication through early enhancement of IFN-I responses.

Highlights

- HIV infection of hu-mice depletes pDC globally and impairs IFN-α production by pDC
- DC expansion by Flt3L suppresses HIV infection in a pDC-dependent manner
- pDC from Flt3L-treated mice are more responsive to TLR7 stimulation
- Early blocking of IFN-I signaling abolishes Flt3L-mediated suppression of viremia

Pham et al., 2019, Cell Reports *29*, 2770–2782
November 26, 2019
https://doi.org/10.1016/j.celrep.2019.10.094

CellPress

OPEN ACCESS
CellPress

Cell Reports
Article

Flt3L-Mediated Expansion of Plasmacytoid Dendritic Cells Suppresses HIV Infection in Humanized Mice

Tram N.Q. Pham,[1,9,*] Oussama Meziane,[1,9] Mohammad Alam Miah,[1,2] Olga Volodina,[1] Chloé Colas,[3] Kathie Béland,[3] Yuanyi Li,[3] Frédéric Dallaire,[1] Tibor Keler,[4] Jean V. Guimond,[5] Sylvie Lesage,[6,7] Cheolho Cheong,[1,7] Élie Haddad,[3,7,8] and Éric A. Cohen[1,7,10,*]

[1]Montréal Clinical Research Institute, Montréal, QC H2W 1R7, Canada
[2]Department of Physiology, Bangladesh Agricultural University, Mymensingh 2202, Bangladesh
[3]Research Center of CHU Sainte-Justine, Montréal, QC H3T 1C5, Canada
[4]Celldex Therapeutics, Hampton, NJ 08827, USA
[5]Centre de Santé et de Services Sociaux Jeanne-Mance, Montreal, QC H2T 1H4, Canada
[6]Department of Immunology-Oncology, Maisonneuve-Rosemont Hospital, Montréal, QC H1T 2M4, Canada
[7]Department of Microbiology, Infectiology and Immunology, Université de Montréal, Montréal, QC H3T 1J4, Canada
[8]Department of Pediatrics, Université de Montréal, Montréal, QC H3T 1J4, Canada
[9]These authors contributed equally
[10]Lead Contact
*Correspondence: tram.pham@ircm.qc.ca (T.N.Q.P.), eric.cohen@ircm.qc.ca (É.A.C.)
https://doi.org/10.1016/j.celrep.2019.10.094

SUMMARY

Plasmacytoid dendritic cells (plasmacytoid DC, pDC) are major IFN-I producers and have been shown to be affected by HIV through ill-defined mechanisms. In this study, we directly assess the role of pDC in early infection, evaluating whether modulating their abundance can alter viral replication. First, HIV infection of humanized mice induces systemic depletion of pDC, and in the presence of soluble FMS-like tyrosine kinase 3 ligand (Flt3L), pDC levels remain elevated. Flt3L significantly delays the onset of viremia and reduces viral replication via a process that is dependent on pDC and mediated through an enhanced early IFN-I response. pDC from Flt3L-treated mice are more prone to express IFN-α following TLR7 stimulation, but this propensity is gradually decreased during infection. In conclusion, maintaining pDC levels and function is key to effective early viral control, and in this context, these findings provide practical insights for anti-HIV strategies and vaccine design.

INTRODUCTION

Plasmacytoid dendritic cells (DC) are main producers of type I interferon (IFN-I) and play an important role in bridging innate and adaptive immunity. Plasmacytoid DC express abundant TLR7 and TLR9, allowing them to recognize respectively, single-stranded RNA (ssRNA) as well as unmethylated DNA with CpG motifs, triggering copious release of IFN-I and other pro-inflammatory cytokines (Swiecki and Colonna, 2015). HIV sensing by pDC occurs predominantly through endosomal recognition of the viral ssRNA by TLR7, and infected cells are reportedly more efficiently sensed than cell-free virions (Beignon et al., 2005; Lepelley et al., 2011). Sensing in early endosomes leads to IFN-I production, whereas that in late endosomes/lysosome promotes release of pro-inflammatory cytokines and co-stimulatory molecules (O'Brien et al., 2011). Human pDC can secrete all types of IFN-I; the most commonly known are IFN-α and IFN-β (Ito et al., 2006).

GS-9620, a TLR7 agonist, can inhibit HIV infection *in vitro* through a mechanism that is dependent on IFN-I produced by pDC (Bam et al., 2016). However, *in vivo*, IFN-I responses can be beneficial or deleterious depending on the timing. Indeed, blocking IFN-I signaling in early weeks of simian immunodeficiency virus (SIV) infection results in accelerated disease progression, and administration of IFN-α2 initially prevents systemic infection in macaques, but further treatment promotes an IFN-tolerant state (Sandler et al., 2014). In chronically infected sooty mangabeys, exogenous IFN-α2 brings about a significant but transient decline in viremia (Vanderford et al., 2012). Nevertheless, during chronic infection, the presence of pDC and sustained IFN production could contribute to HIV-induced immunopathogenesis (Li et al., 2014) because persistent IFN-I signaling is associated with aberrant immune activation, heightened inflammation, accelerated cell death, and dysregulated immune cell function (Cheng et al., 2017; Herbeuval et al., 2005a, 2005b; Li et al., 2017; O'Brien et al., 2013; Zhang et al., 2015; Zhen et al., 2017). Interestingly, the fact that HIV traffics predominantly to early endosomes favors persistent IFN-α production (O'Brien et al., 2011), perpetuating a condition that allows further chronic inflammation and viral persistence. In this regard, IFN-I signaling blockade by an IFN-I receptor antagonist during chronic SIV infection has recently been found to lower inflammation without altering T cell activation/exhaustion or viral replication (Nganou-Makamdop et al., 2018).

The effect of HIV/SIV infection on pDC homeostasis has been documented previously, although it is not clear whether pDC were redistributed or depleted (Barratt-Boyes et al., 2010; Barron et al., 2003; Biancotto et al., 2007; Brown et al., 2009;

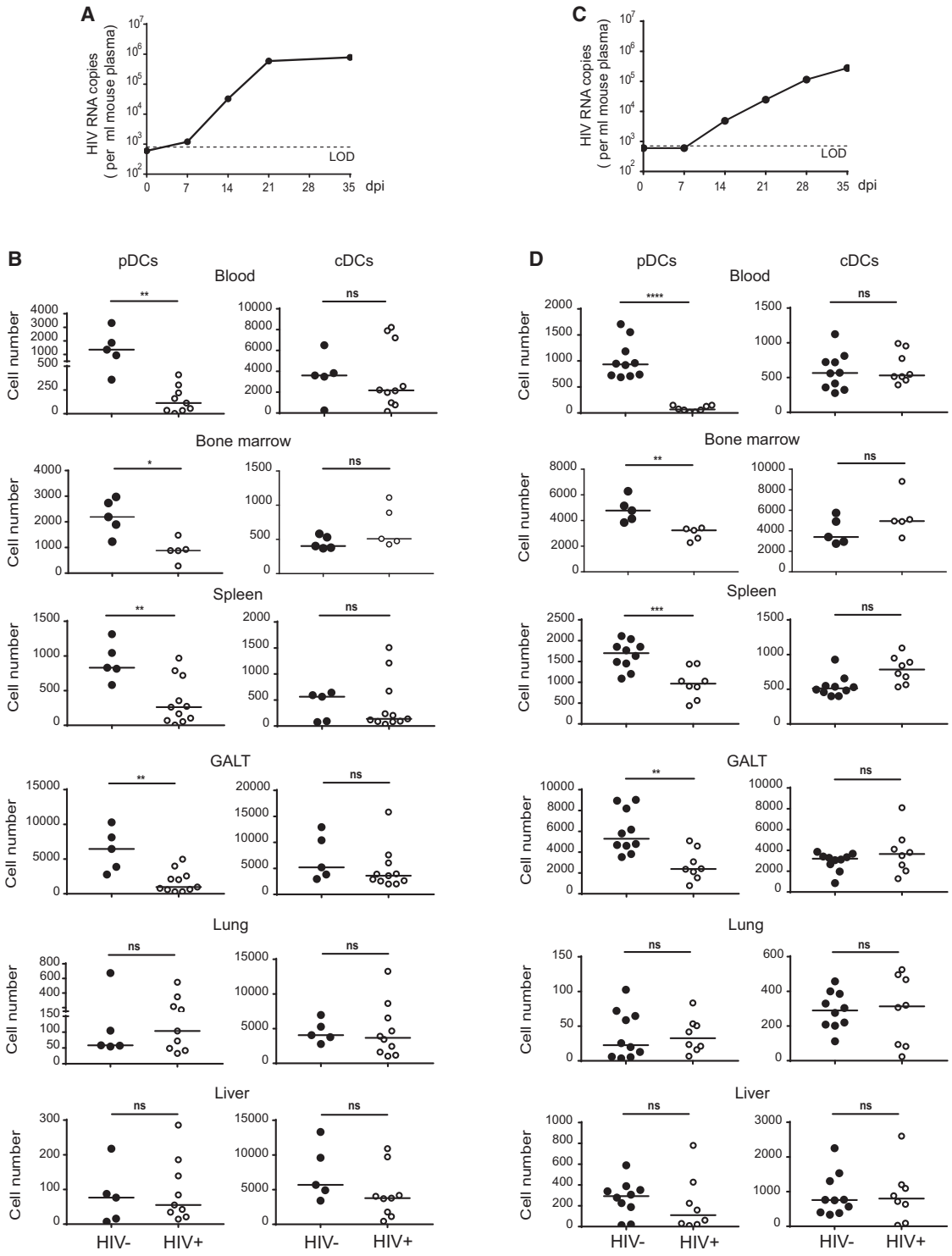

Figure 1. HIV Infection Induces Depletion of pDC in Humanized Mice

(A and B) hNSG mice were infected with CCR5-tropic HIV-1 NL4.3-ADA-GFP virus for up to 35 days. Shown are plasma viral loads (A; at least 10 mice per time point) and DC frequency (B; relative to 10^5 human $CD45^+$ cells) from peripheral blood and the indicated tissues at 21 dpi, as determined by flow cytometry. Each dot represents one mouse, and there were 5–10 mice analyzed per group, as indicated on the graph.

(legend continued on next page)

Donaghy et al., 2001; Kwa et al., 2011; Lehmann et al., 2014; Li et al., 2013; Reeves et al., 2012; Sabado et al., 2010). Indeed, in studies with HIV-infected patients or SIV-infected monkeys, a decreased pDC count in the blood was associated with pDC being accumulated in the colorectum, gut mucosae, or associated draining lymph nodes (LNs) (Lehmann et al., 2014; Li et al., 2013; Reeves et al., 2012). In contrast, other investigations in humans and animals have documented a loss of pDC in the blood and LNs (Barratt-Boyes et al., 2010; Barron et al., 2003; Biancotto et al., 2007; Brown et al., 2009; Donaghy et al., 2001; Sabado et al., 2010). It is unlikely that the depletion is a direct effect of the virus on the cells because pDC are largely not susceptible to productive infection owing to high level expression of endogenous restriction factors such as SAMHD1 (Bloch et al., 2014).

As mentioned above, robust IFN-I responses are important in early control of HIV/SIV infection, suggesting a beneficial role of pDC. Nevertheless, cellular factors, including chemokines produced by SIV-activated pDC, can reportedly recruit target cells to initial sites of viral invasion, effectively establishing the infection (Li et al., 2009). This paradox implies that spatio-temporal modulation of pDC location and function could conceivably enhance antiviral responses without inciting heightened, detrimental immune activation. In this study, we directly assessed the role of pDC during early HIV infection in humanized mice, determining whether modulating pDC levels *in vivo* would shape the course of viral replication. We found that HIV infection induced systemic depletion of pDC in the periphery and lymphoid tissues. Interestingly, global expansion of DC by CDX-301, a soluble form of Flt3L, led to a significant delay in HIV infection and meaningful reduction of viremia in humanized mice. Importantly, this antiviral effect of Flt3L was dependent on pDC and mediated through an enhanced IFN-I response because blocking this pathway relieved the viral control by Flt3L. Intriguingly, pDC mobilized by Flt3L were more responsive to TLR7 stimulation, although their ability to make IFN-α was gradually reduced over the course of infection. Overall, our findings clearly demonstrate a protective role of pDC in early stages of infection, providing a potential rationale for future development of pDC-based therapeutic approaches to complement conventional anti-HIV strategies.

RESULTS

HIV Infection Induces Depletion of pDCs in Humanized Mice

We first assessed the effect of HIV infection on pDC during early infection using humanized mouse models. In this system of humanized non-obese diabetic (NOD)-severe combined immunodeficiency (SCID) IL2Rγ^{null} (hNSG) mice, viremia levels began to plateau around 21 days post infection (21 dpi) (Figure 1A). Because the aim was to study the role of pDC in the early phases, 21 dpi was usually the endpoint in subsequent experiments. Flow cytometry (Figure S1) was used to assess the effect of HIV on pDC homeostasis. At 21 dpi, we observed a significant decrease in pDC frequency, albeit to varying extents between the blood, bone marrow (BM), spleen, and gut-associated lymphoid tissues (GALT) (Figure 1B). Indeed, pDC were decreased by 10-fold in the blood, whereas those in the tissues were reduced by approximately 3- to 5-fold. Notably, there was no concomitant increase in pDC levels in the lungs and liver (Figure 1B), suggesting that HIV primarily induces depletion of pDC in hNSG mice. In sharp contrast, conventional DCs (cDC) were largely unaffected by HIV.

To ascertain whether the presence of both innate and adaptive immunity would influence the extent of pDC depletion by HIV, we performed similar experiments in humanized Bone Marrow Liver Thymus (hBLT) mice (Marsden and Zack, 2017) and found comparable viral kinetics as well as similar effects of HIV on pDC (Figures 1C and 1D). In both models, pDC levels were reduced to a greater extent in the blood than in the BM, spleen, or GALT. We speculate that the more profound decrease in pDC in the blood could have been a combination of cell depletion by HIV and homeostatic mobilization to tissues during infection.

Flt3L Treatment Reduces HIV Infection in Humanized Mice

Given that pDC were greatly decreased in early HIV infection, we asked whether expanding this population *in vivo* could alter the course of HIV replication. As documented previously, we found that a soluble form of Flt3L, CDX-301, induced a marked systemic increase in DC frequencies in the blood and tissue without having a discernable effect on T cells or monocytes (Anandasabapathy et al., 2015; Masten et al., 2004; Pulendran et al., 2000; Figure S2). Of note, although cDC were expanded by about 2-fold in the blood, spleen, GALT, and BM, pDC levels were significantly higher (up to 5-fold) in these compartments. Moreover, pDC in non-lymphoid tissues of the lungs and liver were enhanced by at least 10-fold following Flt3L treatment, whereas cDC levels were not significantly affected (Figure S2). Similar frequencies of pDC were obtained when CD123$^+$ cells (Figure S1A) were gated on CD4, BDCA2, or ILT7 (Figures S1B and Figure S2C). In the context of uninterrupted Flt3L treatment, when mice were challenged with the NL4.3-ADA virus (Figure 2A), we observed nearly complete protection from HIV infection at 7 dpi (Figure 2B). At 14 dpi, viral loads (VL) were almost 2-log lower in the Flt3L-treated group, and the reduced viremia was maintained throughout the follow-up. Additionally, in tissues of Flt3L-treated mice (BM, spleen, lungs, and liver), we observed a markedly lowered level of cells carrying the integrated HIV DNA genomes (Figures 2C–2E) or expressing viral proteins (p24$^+$). Importantly, this protective effect of Flt3L was sustained over 35 days of infection (Figure 2F), demonstrating a long-lasting effect of Flt3L. The fact that Flt3L treatment enabled similar control of HIV infection in

(C and D) The same experimental design and analysis as in (A) and (B) but for hBLT mice. (C) has 9 mice per time point. (D) has 5–10 mice per group, as indicated on graph. Each dot represents one mouse.
Horizontal lines indicate median values. Statistical analysis: two-tailed Mann-Whitney tests; ns, not significant; *p < 0.05, **p < 0.01, ***p < 0.001, ****p < 0.0001. LOD, limit of detection. See also Figure S1 and Table S1.

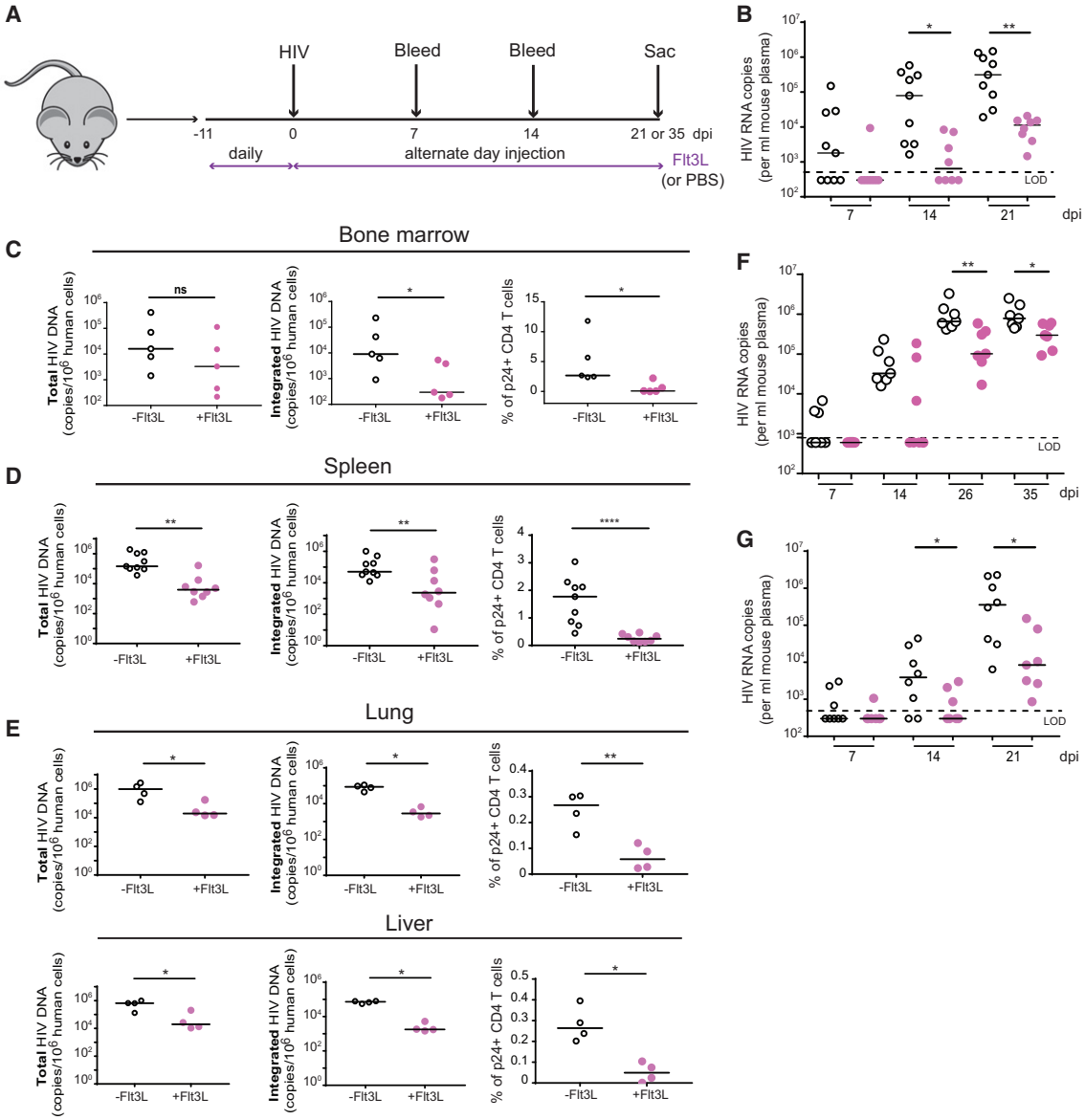

Figure 2. Flt3L Treatment Reduces HIV Infection in Humanized Mice

(A) Experimental setup to evaluate the effect of Flt3L treatment on HIV infection in hNSG and hBLT mice.

(B) Plasma viral loads over a 21-day infection period in hNSG mice receiving PBS (black circles, 9 mice) or Flt3L (purple, 8 mice).

(C–E) Total and integrated HIV DNA was quantified by real-time PCR in BM (C) (5 mice per group), spleen (D) (9 mice in the PBS group, 8 mice in the Flt3L group), and (E) lungs (4 mice per group) and liver (4 mice per group) at 21 dpi. Frequencies of HIV-infected ($p24^+$) $CD4^+$ T cells were determined by flow cytometry.

(F) Plasma viral loads over a 35-day infection period in hNSG mice receiving PBS (black circles, 7 mice) or Flt3L (purple, 7 mice).

(G) Plasma viral loads over a 21-day infection period in hBLT mice receiving PBS (black circles, 8 mice) or Flt3L (purple, 7 mice).

Each dot represents one mouse. In (B)–(G), horizontal lines indicate median values. Statistical analysis: two-tailed Mann-Whitney tests; *$p < 0.05$, **$p < 0.01$, ****$p < 0.0001$. See also Figures S2–S4 and Table S1.

hBLT mice suggested that the protective role of Flt3L was not altered by the presence of a concomitant adaptive immune response (Figure 2G). Further, we examined the effect of Flt3L on infection with the transmitted founder virus CHO77 and found similar control of HIV replication (Figure S3). However, in the context of a potential therapeutic application for Flt3L, when viral propagation had already reached a chronic set-point level, initiating expansion of pDC did not lead to a reduction in viremia (Figure S4).

We next investigated the effect of uninterrupted Flt3L injections on pDC levels during HIV infection and found that their levels in the blood and tissues remained persistently elevated in infected animals (Figure 3). Flt3L modestly expanded cDC, and in agreement with data shown previously (Figure 1),

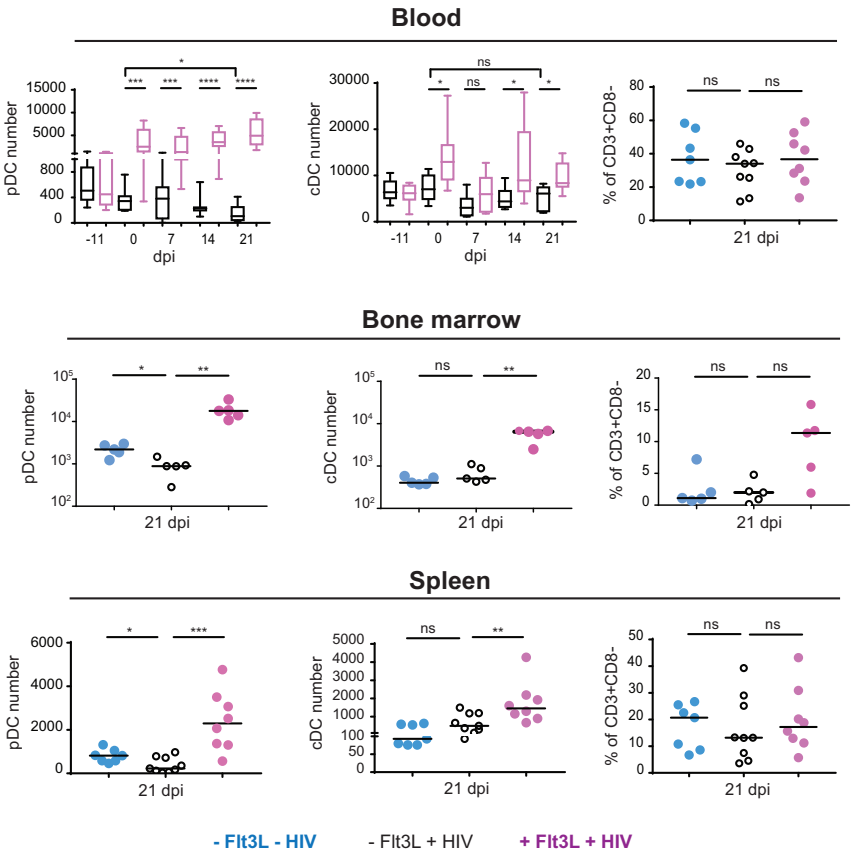

Figure 3. Flt3L Treatment Helps Maintain pDC Levels during HIV Infection

hNSG mice were administered PBS or Flt3L and infected with CCR5-tropic HIV-1 NL4-3.ADA-GFP virus as depicted in Figure 2A. Shown are frequencies of DC and CD4$^+$ T cells in the blood (7 mice in uninfected −Flt3L−HIV, 9 mice in −Flt3L+HIV, and 8 mice in +Flt3L+HIV), bone marrow (5 mice per group), and spleen (7 mice in −Flt3L−HIV, 9 mice in −Flt3L+HIV, and 8 mice in +Flt3L+HIV), as determined by flow cytometry. Box-and-whisker plots highlight minimum, maximum, and median values. Horizontal lines on scatter dot plots indicate median values. Each dot represents a mouse. Statistical analysis: two-tailed Mann-Whitney tests; *p < 0.05, **p < 0.01, ***p < 0.001, ****p < 0.0001. See also Figure S1 and Table S1.

cDC were not affected by HIV. As reportedly previously, CD4$^+$ T cell levels remained constant over 21-day infection with the NL4.3-ADA virus (Dave et al., 2013), and Flt3L treatment did not alter their frequency, except in the BM, where CD4$^+$ T cells were evidently increased, albeit this was statistically insignificant. Nevertheless, despite this trend, HIV infection in this organ was still reduced compared with BM from Flt3L-untreated mice (Figure 2C). Taken together, our findings indicate that Flt3L administration prior to and during infection significantly delayed HIV infection and lowered the frequencies of infected cells, a phenomenon that was intimately associated with elevated levels of pDC.

Flt3L Treatment Reduces HIV Replication via a Process that Is Dependent on pDC

To directly prove that Flt3L-mediated control of HIV replication was a consequence of pDC expansion, we used a pDC-specific monoclonal antibody (mAb) to deplete this population from hNSG mice and monitored the effect of this depletion on viral replication (Figure 4A). 15B is an anti-BDCA2 mAb that has been shown to efficiently remove pDC from the blood and tissues of humanized mice (Li et al., 2014). To this end, we found that, although Flt3L led to a pronounced decrease in viremia (median by 1.6 log) (Figure 4B), Ab-mediated depletion of pDC (Figure 4C) restored viremia to the level of untreated mice, effectively abolishing the Flt3L effect (Figure 4B). Accordingly, the frequencies of splenocytes carrying HIV genomes (Figure 4D) or CD4$^+$ T cells actively expressing viral proteins (p24$^+$) (Figure 4E) were comparable between Flt3L-untreated and pDC-depleted, Flt3L-treated groups. These data confirm the involvement of pDC in Flt3L-mediated control of HIV replication. As expected, cDC were not affected by 15B (Figure 4C), confirming the specificity of depletion (Li et al., 2014) and likely excluding an essential, direct role of cDC. Overall, our data clearly demonstrate that Flt3L treatment leads to control of HIV replication via a process that is entirely dependent on pDCs, reaffirming the protective role of pDC during early infection. Indeed, in the absence of Flt3L, pDC depletion by 15B increased viremia by 7.4-fold (median 48,400 versus 6560 copies/mL) as early as 7 dpi (Figures S5A and S5B). Interestingly, this viremic difference became less pronounced over time (4.8-fold difference at 14 dpi and 2.6-fold at 21 dpi), most probably because pDC were being depleted simultaneously by HIV (Figure S4B, right panel). Also, in the context of hBLT mice, pDC depletion by 15B abolished viremic suppression induced by Flt3L (Figure S5C). Interestingly, unlike earlier findings in hNSG mice (Figure 4B-C), viral loads in the 15B-treated group were higher than in the Flt3L-untreated group (median, 11,2640 versus 33,760) and correlated with a reduced pDC level (215 versus 488 cells in 10^5 hCD45$^+$) (Figures S5C and S5D). Taken together, these findings not only reaffirm the intimate relationship between pDC abundance and viremia but also underline the benefit of expanding pDC via Flt3L treatment to maintain viral control.

Flt3L-Derived pDCs Are More Prone to Express IFN-α following TLR7 Stimulation

Given that Flt3L-mediated expansion of pDC reduced HIV infection, we asked whether pDC generated by Flt3L were functionally different from those at steady state. First, we found that pDC from Flt3L-treated mice were more responsive to *ex vivo* stimulation with the TLR7 agonist R848, as shown by a

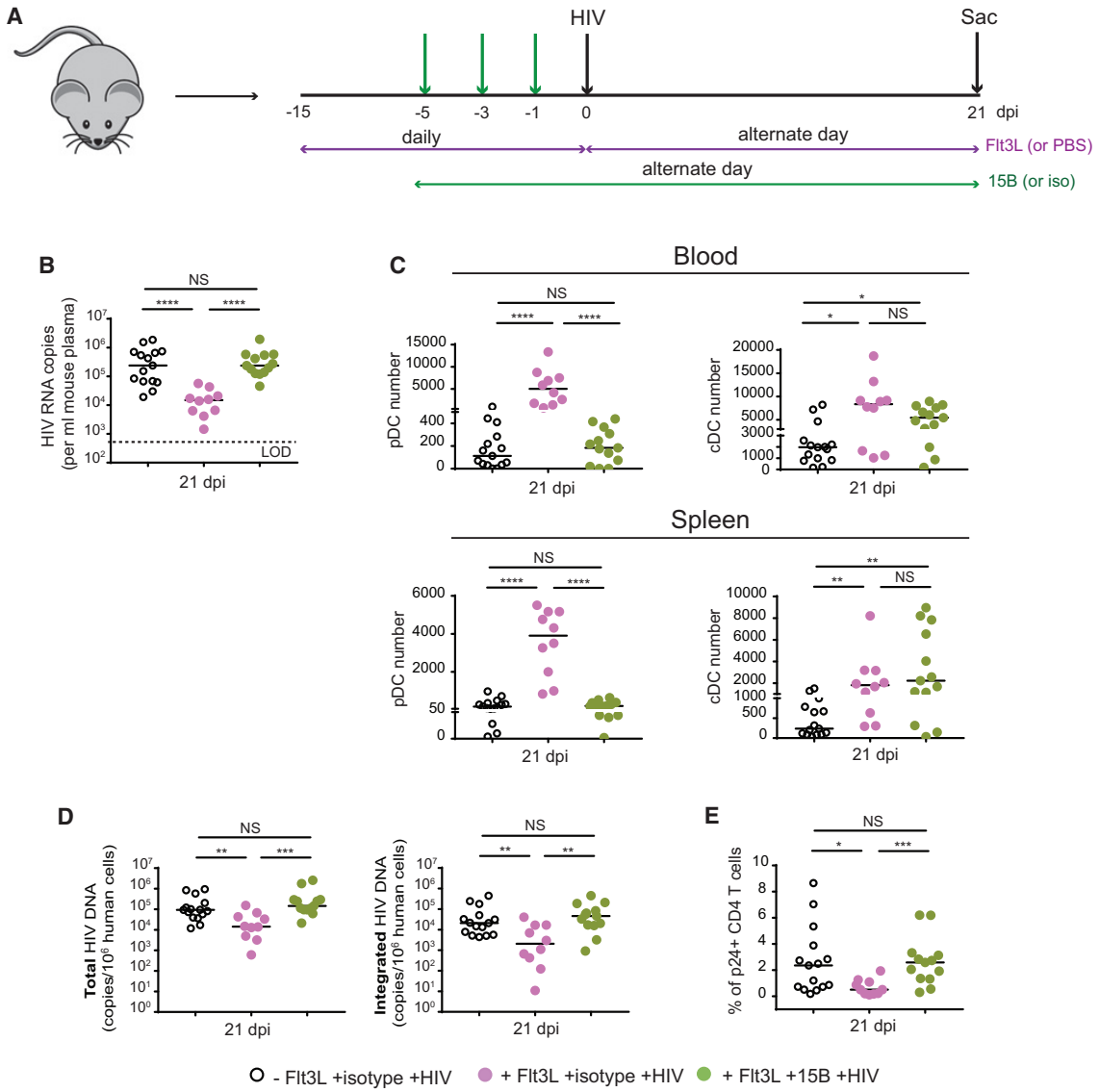

Figure 4. Flt3L Treatment Reduces HIV Replication via a pDC-Dependent Process

(A) Experimental setup to determine whether Flt3L-mediated control of HIV infection is driven by pDC. hNSG mice were administered PBS or Flt3L as shown and subsequently received three injections of the pDC-specific Ab 15B or an isotype control. Mice were then infected with CCR5-tropic HIV-1 NL4-3.ADA.GFP.

(B) Plasma viral load at sacrifice.

(C) DC levels in the blood and spleen.

(D) Total and integrated HIV DNA in the spleen.

(E) Frequency of HIV-infected ($p24^+$) $CD4^+$ T cells in the spleen.

Each dot represents a mouse. Horizontal lines indicate median values. In (B)–(E), there were 15 mice in −Flt3L+HIV; 10 mice in +Flt3L+iso+HIV, and 13 mice in +Flt3L+15B+HIV. Statistical analysis: two-tailed Mann-Whitney tests; *$p < 0.05$, **$p < 0.01$, ***$p < 0.001$, ****$p < 0.0001$. See also Figures S1 and S5 and Table S1.

higher frequency of IFN-α-expressing cells and, perhaps to a lesser extent, of tumor necrosis factor alpha (TNF-α)-expressing pDC (Figure 5A). When HIV-infected $CD4^+$ T cells were used as a stimulus to mimic a more physiological setting, we noted a similar trend for IFN-α, validating the results with R848 (Figure 5B). In the case of TNF-α, we did not observe a difference between Flt3L-treated and untreated groups (Figure 5B), perhaps suggesting that, in the context of sensing of infected T cells, aside from TLR7 signaling, there may be additional events that regulate TNF-α expression in pDC. Indeed, Webster et al. (2018) showed that pDC sensing of arbovirus-infected cells induces an IRF7-restricted response, favoring IFN-I production but not nuclear factor κB (NF-κB)-mediated inflammatory cytokines such as TNF-α.

At steady state, HLA DR, and CD40 were markedly lower on pDC from Flt3L-treated mice, perhaps reflecting their less

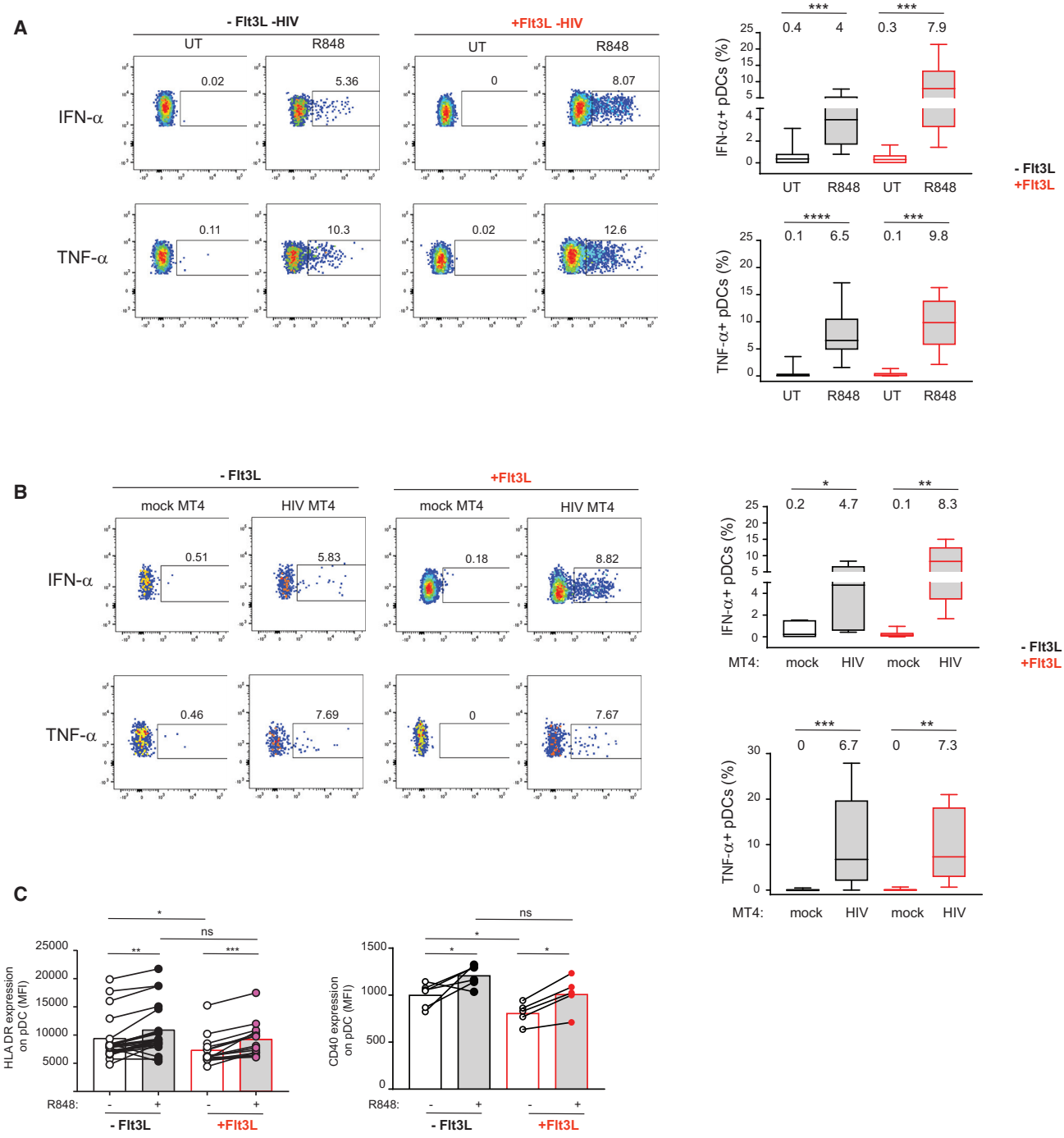

Figure 5. pDC from Flt3L-Treated Mice Are More Prone to Express IFN-α following TLR7 Stimulation *Ex Vivo*

Splenocytes from uninfected hNSG mice treated or not treated with Flt3L were stimulated with an R848 agonist (A) or HIV-infected MT4 cells (B). Unstimulated splenocytes or those cultured with mock-infected MT4 served as controls.

(A and B) Left panels: pseudo-color flow graphs of representative mice showing frequencies of pDC expressing IFN-α or TNF-α. Right panels: pDC capacity to express IFN-α or TNF-α following stimulation in different mice. In the analysis with R848, there were 12 mice per group. In the analysis with HIV-infected MT4 cells, there were 7 mice in the −Flt3L group and 11 mice in the +Flt3L group. Plasmacytoid DC are defined as $mCD45^{-}hCD45^{+}CD3^{-}CD14^{-}CD19^{-}HLADR^{+}CD123^{+}CD11c^{-}CD4^{+}BDCA2^{+}$. Box-and-whisker plots highlight minimum, maximum, and median frequencies of cytokine-expressing pDC. Numbers shown on bar graphs indicate median levels. Statistical analysis: two-tailed Mann-Whitney tests; *$p < 0.05$, **$p < 0.01$, ***$p < 0.001$, ****$p < 0.0001$.

(legend continued on next page)

mature and/or activated status. Nevertheless, in response to stimulation, pDC from both groups expressed comparably elevated levels of the markers, indicating that pDC were indeed activated (Figure 5C).

pDC Capacity to Sense and Make IFN-α Decreases during HIV Infection

Given the results with uninfected mice (Figure 5) and the fact that HIV-1 represses IFN-I responses by exploiting the cross-talk between the restriction factor BST2 and the pDC-inhibitory receptor ILT7 (Bego et al., 2015), we shifted our focus toward furthering our understanding of how IFN-I responses by pDC might be affected in the context of Flt3L. In HIV-infected mice from both Flt3L-treated and untreated groups, we observed a reduction in the level of pDC capable of expressing IFN-α, and this was especially evident at 21 dpi. Nevertheless, at all time points throughout the infection, pDC from Flt3L-treated mice remained more capable of expressing IFN-α than their counterparts from animals not treated with Flt3L (Figures 6A and 6B). Interestingly, the decrease in pDC capacity to make IFNα during HIV infection was likely unrelated to activation status because HLA DR was indiscriminately upregulated on R848-stimulated pDC from both groups and at all time points (Figure 6C), Additionally, we did not observe significant proliferation by pDC in uninfected and infected mice before or after TLR7 stimulation (Figure S6). Importantly, there was no significant difference in the level of $Ki67^+$ pDC before infection and 21 days post infection (Figure S6). Overall, these findings suggest that Flt3L treatment enhances pDC quantitatively and qualitatively and that modulating pDC function may be advantageous for the virus to establish systemic and chronic infection.

Blocking IFN-I Signaling Early Abrogates Flt3L-Mediated Control of HIV Replication

To gain insight into whether the protective effect of Flt3L was specifically mediated through an enhanced IFN-I response, we measured plasma IFN-I over time and assessed whether there was a correlation with viral loads. At 7 dpi, we found no evidence of detectable IFN-I despite observing a reduction in viremia in the Flt3L-treated, isotype control (iso) group compared to the Flt3L-untreated group (Flt3L−). However, at 14 and 21 dpi, we observed a positive correlation between IFN-I release and viremia (Figures 7A and 7B), suggesting that the Flt3L effect could not have been attributed to the increased IFN-I levels sustained throughout the infection. The fact that IFN-I was more readily detectable in the Flt3L-untreated, highly viremic group compared with the Flt3L-treated, virally attenuated group further supports this notion. Unsurprisingly, pDC depletion by 15B suppressed IFN-I release, reaffirming that pDC were the primary source of IFN-I in early infection, as shown previously (Bruel et al., 2014; Li et al., 2014). Also, consistent with findings shown in Figure 4, Ab-mediated depletion of pDC restored viremia to the level of the Flt3L-untreated group (Figure 7A), reaffirming the importance of pDC in viral suppression mediated by Flt3L.

Because viral replication can influence the extent of pDC sensing, which, in turn, modulates IFN-I release (Saïdi et al., 2016; Wimmers et al., 2018), examining IFN-I response at an earlier time point might allow a more accurate determination of its involvement in Flt3L-induced control of HIV infection. Additionally, measuring plasma IFN-I may not necessarily recapitulate the response in tissues. Thus, we evaluated mRNAs of IFN-stimulated genes (ISGs) in splenocytes at 7, 14, and 21 dpi and observed notably higher levels of the ISGs *OAS1*, *Mx1*, and *IRF7* in Flt3L-treated mice at 7 dpi (Figure 7C), suggesting an enhanced IFN-I response during the period of viremic control in Flt3L-treated mice. Interestingly, at 14 dpi, when viremia remained reduced in the Flt3L group, ISG mRNA levels became comparable between the two groups (Figure 7D), implying that, as HIV replication was progressing, the enhanced antiviral IFN-I response elicited initially in the Flt3L group might be diminished by the host's reaction to ongoing viral propagation. Indeed, at 21 dpi, the ISG levels were significantly higher in Flt3L-untreated mice (Figure 7E). In light of these findings, we performed an experiment to determine whether blocking IFN-I signaling early (Zhen et al., 2017) would alter the protective effect of Flt3L. Following confirmation of the neutralizing activity of the anti-IFNAR2 Ab *in vivo* (Figure S7), we treated animals with the Ab prior to HIV challenge and found that blocking IFN-I signaling fully abolished Flt3L-mediated suppression of viremia (Figure 7F). Overall, the findings demonstrate that Flt3L-induced expansion of pDC provides early control against HIV by enhancing IFN-I responses.

DISCUSSION

Plasmacytoid DC play a complex role in HIV infection, potentially having both beneficial and undesirable effects on the immune system. Here we provide direct evidence demonstrating a protective role of pDC in early phases of HIV infection. Specifically, *in vivo* treatment with Flt3L, a cytokine that induces expansion and mobilization of DC subsets (Anandasabapathy et al., 2015; Masten et al., 2004; Pulendran et al., 2000), leads to a significant delay in HIV infection and reduces viral replication through a process that is strictly dependent on pDC. We find that Flt3L-generated pDC are more responsive to TLR7 stimulation, although the pDC capacity to make IFN-α was decreased during infection. Finally, the protective effect of Flt3L is invariably associated with sustained pDC levels and mediated through enhanced IFN-I responses.

We show that HIV infection induces widespread depletion of pDC in the blood and tissues (Figure 1). Loss of blood pDC has been observed previously, and in some studies, the decrease was attributed to pDC redistribution to lymphoid tissues

(C) HLA DR and CD40 expression on pDC before and after stimulation. Expression is depicted as median fluorescence intensity (MFI) from flow graphs. For HLA DR analysis, there were 18 mice in the −Flt3L group and 14 mice in the +Flt3L group. For CD40 analysis, there were 6 mice in the −Flt3L group and 5 mice in the +Flt3L group.

Statistical analysis: Mann-Whitney test to compare differences among treatment groups (A–C) and two-tailed Wilcoxon matched-pairs rank test to compare differences before and after stimulation within the same mouse (C). See also Figure S1 and Table S1.

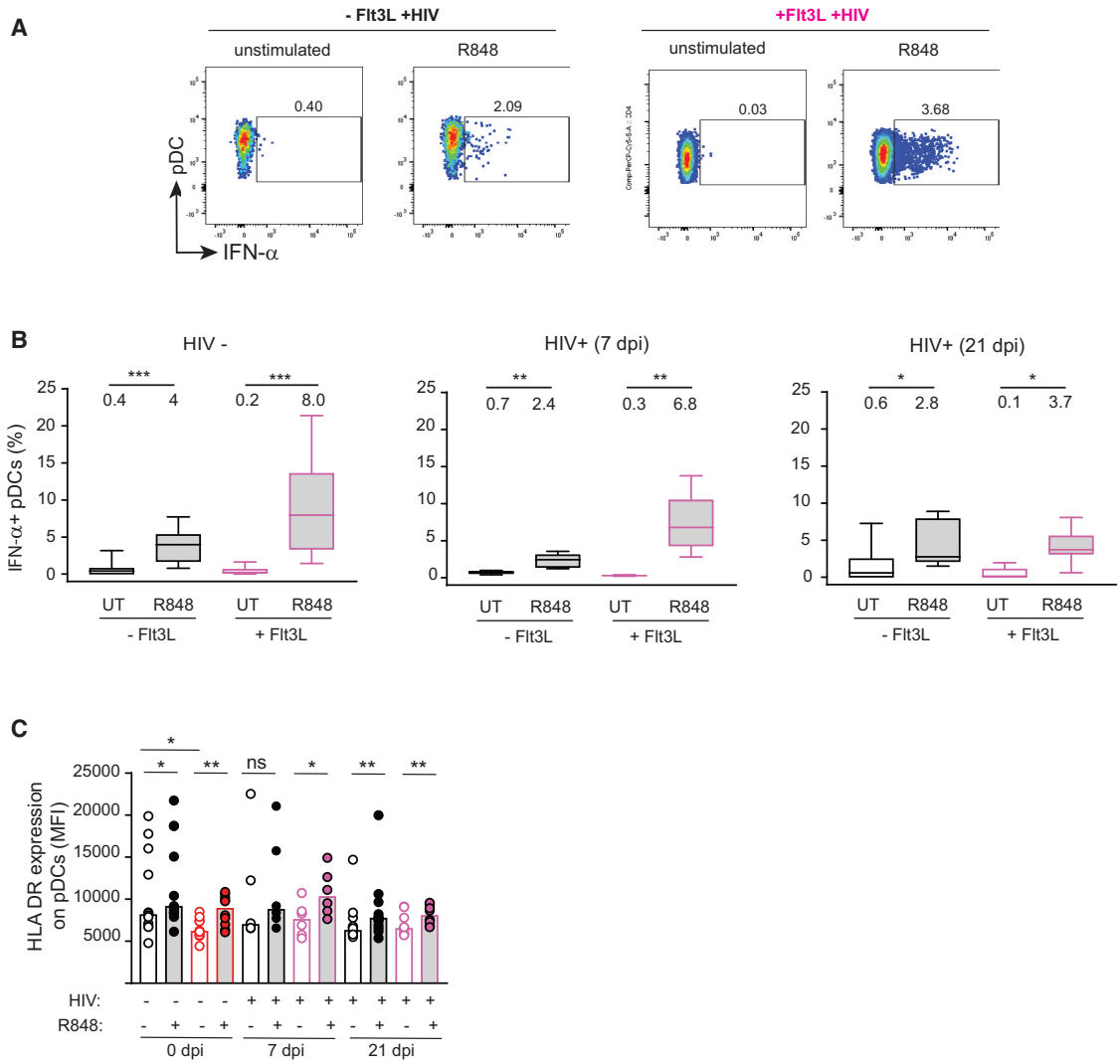

Figure 6. pDC Ability to Make IFN-α in Response to TLR7 Stimulation Is Decreased during HIV Infection

Splenic pDC from HIV-infected mice were analyzed for their ability to make IFN-α following R848 stimulation. Infected and uninfected mice received the same number of Flt3L injections at the time of *ex vivo* analysis.

(A) Representative flow plots showing the frequency of IFN-α-expressing pDC at 21 dpi.

(B) Box-and-whisker plots of IFN-α production by pDC at different time points during infection. Minimum, maximum, and median values are as indicated. There were 10 mice per group for uninfected animals, 6 mice per group for 7 dpi, and 9 mice per group for 21 dpi. Numbers shown on top indicate median frequencies of cytokine-expressing pDC. Statistical analysis: two-tailed Mann-Whitney tests; *$p < 0.05$, **$p < 0.01$, ***$p < 0.001$.

(C) Effect of TLR7 stimulation on HLA DR expression on pDC over the course of infection. Shown are MFIs. There were 10 mice per group for uninfected animals, 6 mice per group for 7 dpi, and 9 mice per group for 21 dpi. See also Figures S1 and S6 and Table S1. Refer also to the Figure 5 legend for the definition of pDC.

(Barratt-Boyes et al., 2010; Barron et al., 2003; Biancotto et al., 2007; Brown et al., 2009; Donaghy et al., 2001; Kwa et al., 2011; Lehmann et al., 2014; Li et al., 2013; Reeves et al., 2012; Sabado et al., 2010). It is currently unclear whether the loss is due to reduced production of pDC progenitors from the BM, as demonstrated in lymphocytic choriomeningitis (LCMV) infection (Macal et al., 2018), or due to apoptosis (Brown et al., 2009; O'Brien et al., 2013). In the latter context, the nature of lymphoid tissue architecture in hNSG mice might affect pDC's ability to recirculate, favoring a microenvironment conducive to apoptosis (Swiecki et al., 2011).

Interestingly, uninterrupted Flt3L treatment was invariably associated with reduced viremia and sustained pDC levels throughout infection (Figures 2 and 3). Importantly, the effect of Flt3L on viral replication was observed with both laboratory-adapted and transmitted founder viral strains. The fact that Flt3L-mediated control was completely abrogated when pDC were depleted unequivocally demonstrates that the protection was mediated by pDC (Figure 4), although we cannot fully exclude potential indirect involvement of other cell types. Consistent with findings in rodents (Björck, 2001), splenic pDC from Flt3L-treated mice were more responsive to stimulation

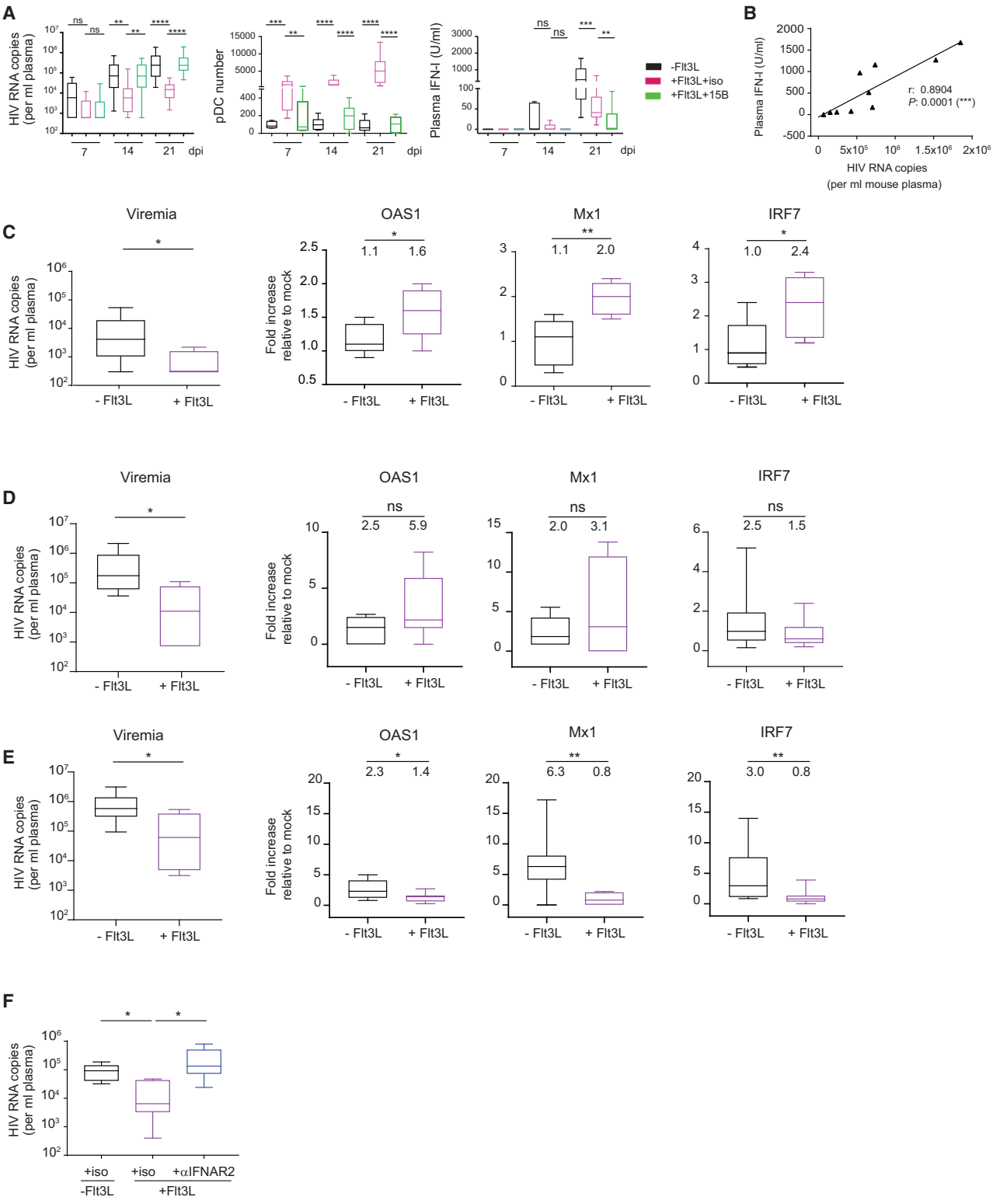

Figure 7. Flt3L-Mediated Control of HIV Replication Is Driven by Early Enhancement of IFN-I Responses

(A) Design of the experiment as described for Figure 4. Plasma viral loads as well as coordinated measurements of pDC frequency and IFN-I were quantified at 7, 14, and 21 dpi. For the analyses of VLs and pDC frequency at 7 dpi, there were 12 mice in the −Flt3L group, 9 mice in +Flt3L+iso, and 12 mice in +Flt3L+15B. At 14 dpi, 12 mice in each group were analyzed for VLs and pDC frequency. At 21 dpi, there were 15 mice in the −Flt3L+HIV group, 10 mice in +Flt3L+iso+HIV group,

(legend continued on next page)

with both the TLR7 agonist R848 and HIV-infected T cells, as shown by a higher frequency of IFN-α-expressing pDCs (Figure 5). Nevertheless, their capacity to make IFN-α was gradually decreased during infection, with fewer pDC expressing IFN-α at 21 dpi compared with 7 dpi. We hypothesize that IFN-I response by pDC is essential to maintain the protective effect of Flt3L and, consequently, the reduction might diminish the effectiveness of Flt3L treatment over time. Indeed, viral loads were elevated at 21 dpi compared with 7 dpi, despite the fact that pDC levels were similar at both time points. The ability of HIV to modulate pDC function is consistent with previous reports documenting pDC dysfunction in early infection. Indeed, Huang et al. (2011) observed a significant decrease in the frequency of IFN-α-expressing pDC in response to an R848-like TLR7 agonist in patients with acute HIV infection. Along this line, in monkeys with acute SIV infection, activation-induced exhaustion of pDC and/or expansion of non-functional pDC precursors blunts their responsiveness to viral stimulation (Bruel et al., 2014). Further, the notion of a gradual decrease in pDC function following viral infection is not restricted to HIV or SIV infection. In fact, it has been reported in a chronic model of LCMV that the ability of pDC to produce IFN-α progressively decreased as early as 5 dpi, and the defect was maintained over the 30-day follow-up (Macal et al., 2018).

Although plasma IFN-α was not detectable in the first 7 days of infection, we show that the protective effect of Flt3L was driven by an early, enhanced IFN-I response because blocking of IFN-I signaling abolished suppression of viremia; we also observed higher ISG levels in tissue at 7 dpi in Flt3L-treated mice. Nevertheless, over the course of infection, it became evident that plasma IFN-I or tissue ISGs could not be predictive/correlated measures of viral control (Figure 7). It is possible that different IFN-I subtypes might have been released unequally, and perhaps those with anti-HIV activity were not as abundant as the others. Indeed, HIV-activated pDC produce IFN-I subtypes with weaker antiviral properties more plentifully (Harper et al., 2015). Also, IFN-I production is regulated through an autocrine/paracrine loop (Wimmers et al., 2018), and HIV enhances IFN-I release in a concentration-dependent manner (Saïdi et al., 2016) In this context, the positive correlation between viremia and IFN-I at 21 dpi is analogous to what has been observed previously within the first 10 days of infection in macaques (Bruel et al., 2014). Consequently, reduced viral replication in Flt3L-treated animals could conceivably lead to less IFN-I being produced, which, in turn, could affect ISG levels, as evident in our study.

Taken together, our findings clearly demonstrate the protective role of pDC during early HIV infection and provide important insights toward furthering our understanding of critical events that govern viral transmission, systemic viral dissemination, and establishment of persistent long-lived viral reservoirs (Li et al., 2009; Sandler et al., 2014). As shown in this study, the progressive loss of pDC sensing capacity coupled with systemic depletion of pDC following HIV infection highlights a potential need for development of therapeutic approaches that help maintain pDC function to ultimately allow a more robust innate immune response against HIV.

STAR★METHODS

Detailed methods are provided in the online version of this paper and include the following:

- KEY RESOURCES TABLE
- LEAD CONTACT AND MATERIALS AVAILABILITY
- EXPERIMENTAL MODEL AND SUBJECT DETAILS
  - Humanized NSG and BLT mice
  - Cell lines
  - Measurements of bioactive IFN-I using HEK-Blue IFN-α/β reporter cells
  - Primary cell cultures: *ex vivo* stimulation of splenocytes with HIV-infected CD4$^+$ T cells and TLR7/8 agonist Resiquimod R848
- METHOD DETAILS
  - Virus production
  - Flt3L treatment, infection of humanized mice and quantification of viral loads
  - Depletion of human pDC and blocking of type I IFN (IFN-I) signaling
  - Cell isolation from peripheral blood and tissues
  - Flow cytometry
  - Nucleic acid extraction and quantification of HIV genomes and human genes by real-time PCR
- QUANTIFICATION AND STATISTICAL ANALYSIS
- DATA AND CODE AVAILABILITY

SUPPLEMENTAL INFORMATION

Supplemental Information can be found online at https://doi.org/10.1016/j.celrep.2019.10.094.

ACKNOWLEDGMENTS

We thank Dr. Liguo Zhang (Institute of Biophysics, Chinese Academy of Sciences, Beijing) for the generous gift of the 15B Ab. The following reagents were obtained through the NIH AIDS Reagent Program, Division of AIDS, NIAID, NIH: ACH-2 cells from Dr. Thomas Folks (catalog number 349), MT4 cells from Dr. Douglas Richman (catalog number 120), CEM.NKR-CCR5+ CD4$^+$ T from Dr. Alexandra Trkola, and HelaTZMbl cells from Drs. John C.

and 13 mice in the +Flt3L+15B+HIV group. For the analysis of IFN-I, there were 7 mice per group for 7 dpi, 6 mice per group for 14 dpi, and 18 mice per group for 21 dpi. For each sample, the IFN-I assay was done in biological duplicates.

(B) Pearson correlation analysis was performed to determine whether plasma IFN-I and HIV viremia (21 dpi) were correlated (Pearson r, 0.8904; *P*, 0.0001). Each point represents a mouse (11 mice analyzed).

(C–E) hNSG were infected with HIV-1 NL4-3.ADA-GFP virus. Plasma viral load and mRNA levels of ISGs *OAS1*, *Mx1*, and *IRF7* in splenocytes were evaluated at (C) 7 dpi (6 mice per group), (D) 14 dpi (6 mice per group), and (E) 21 dpi (10 mice for −Flt3L and 8 mice for +Flt3L).

(F) hNSG mice were injected with Flt3L and, 24 h before HIV challenge, treated with αIFNAR2 mAb or isotype control (iso). Flt3L and αIFNAR2 injections were continued for 7 days. Shown is HIV viremia (5 mice per group).

Box-and-whisker plots highlight minimum, maximum, and median values. Statistical analysis: two-tailed Mann-Whitney tests; *$p < 0.05$, **$p < 0.01$, ***$p < 0.001$, ****$p < 0.0001$. See also Figure S7 and Table S1.

Kappes and Xiaoyun Wu (catalog number 8129). We are grateful to Drs. Nicolas Chomont and Rémi Fromentin (CR-CHUM, Montreal) for guidance and assistance with the qPCR assay to measure HIV genomes. We appreciate the technical support provided by the staff of the animal facilities at the IRCM and CR-Ste Justine as well as the IRCM cytometry platform. We also thank Natacha Patey and Renée Dicaire for assistance with generation of hBLT mice. We are grateful to Mariana Bego and Sabelo Lukhele for helpful discussions and a critical review of the manuscript. We thank Jonathan Boulais for assistance with the graphical abstract. We are thankful to Mélanie Laporte and Jaspreet Jain for assistance with animal work as well as former members of the Cheolho Cheong laboratory for helpful discussions and guidance with animal experimentation. This study was supported by Canadian Institutes of Health Research (CIHR) grants IBC150403 and PJT 153355 (to É.A.C., E.H., and S.L.), a Canadian HIV Cure Enterprise (CanCURE) grant from the CIHR partnership with the Canadian Foundation for AIDS Research and the International AIDS Society (HIG 133050 to É.A.C.), and a grant from the Fonds de Recherche du Québec-Santé AIDS and Infectious Disease Network (to É.A.C.). We dedicate this paper to the memory of our friend and colleague, Dr. Cheolho Cheong, whose dedication to this study will not be forgotten.

AUTHOR CONTRIBUTIONS

T.N.Q.P. designed and performed experiments, analyzed data, and wrote the manuscript. O.M. designed and performed experiments, analyzed data, and assisted with preparation of the manuscript. M.A.M. designed and performed experiments and analyzed data. O.V. performed selected qPCR analyses and assisted with animal experimentation. C.Colas., Y.L., and J.V.G. produced hBLT mice, and K.B. produced hNSG mice. F.D. provided technical assistance. T.K. provided CDX-301 and expertise regarding protocol. S.L. provided expertise and input regarding the conception of the study. E.H. supervised the generation of humanized mice and provided expertise and input regarding the conception of the study. C.Cheong conceived and supervised the study. É.A.C. conceived and supervised the study and wrote the manuscript.

DECLARATION OF INTERESTS

T.K. is an employee and a shareholder of Celldex Therapeutics.

Received: October 28, 2018
Revised: August 29, 2019
Accepted: October 23, 2019
Published: November 26, 2019

REFERENCES

Anandasabapathy, N., Breton, G., Hurley, A., Caskey, M., Trumpfheller, C., Sarma, P., Pring, J., Pack, M., Buckley, N., Matei, I., et al. (2015). Efficacy and safety of CDX-301, recombinant human Flt3L, at expanding dendritic cells and hematopoietic stem cells in healthy human volunteers. Bone Marrow Transplant. *50*, 924–930.

Bam, R.A., Hansen, D., Irrinki, A., Mulato, A., Jones, G.S., Hesselgesser, J., Frey, C.R., Cihlar, T., and Yant, S.R. (2016). TLR7 Agonist GS-9620 Is a Potent Inhibitor of Acute HIV-1 Infection in Human Peripheral Blood Mononuclear Cells. Antimicrob. Agents Chemother. *61*, 61.

Barratt-Boyes, S.M., Wijewardana, V., and Brown, K.N. (2010). In acute pathogenic SIV infection plasmacytoid dendritic cells are depleted from blood and lymph nodes despite mobilization. J. Med. Primatol. *39*, 235–242.

Barron, M.A., Blyveis, N., Palmer, B.E., MaWhinney, S., and Wilson, C.C. (2003). Influence of plasma viremia on defects in number and immunophenotype of blood dendritic cell subsets in human immunodeficiency virus 1-infected individuals. J. Infect. Dis. *187*, 26–37.

Bego, M.G., Côté, É., Aschman, N., Mercier, J., Weissenhorn, W., and Cohen, E.A. (2015). Vpu Exploits the Cross-Talk between BST2 and the ILT7 Receptor to Suppress Anti-HIV-1 Responses by Plasmacytoid Dendritic Cells. PLoS Pathog. *11*, e1005024.

Beignon, A.S., McKenna, K., Skoberne, M., Manches, O., DaSilva, I., Kavanagh, D.G., Larsson, M., Gorelick, R.J., Lifson, J.D., and Bhardwaj, N. (2005). Endocytosis of HIV-1 activates plasmacytoid dendritic cells via Toll-like receptor-viral RNA interactions. J. Clin. Invest. *115*, 3265–3275.

Biancotto, A., Grivel, J.C., Iglehart, S.J., Vanpouille, C., Lisco, A., Sieg, S.F., Debernardo, R., Garate, K., Rodriguez, B., Margolis, L.B., and Lederman, M.M. (2007). Abnormal activation and cytokine spectra in lymph nodes of people chronically infected with HIV-1. Blood *109*, 4272–4279.

Björck, P. (2001). Isolation and characterization of plasmacytoid dendritic cells from Flt3 ligand and granulocyte-macrophage colony-stimulating factor-treated mice. Blood *98*, 3520–3526.

Bloch, N., O'Brien, M., Norton, T.D., Polsky, S.B., Bhardwaj, N., and Landau, N.R. (2014). HIV type 1 infection of plasmacytoid and myeloid dendritic cells is restricted by high levels of SAMHD1 and cannot be counteracted by Vpx. AIDS Res. Hum. Retroviruses *30*, 195–203.

Brown, K.N., Wijewardana, V., Liu, X., and Barratt-Boyes, S.M. (2009). Rapid influx and death of plasmacytoid dendritic cells in lymph nodes mediate depletion in acute simian immunodeficiency virus infection. PLoS Pathog. *5*, e1000413.

Bruel, T., Dupuy, S., Démoulins, T., Rogez-Kreuz, C., Dutrieux, J., Corneau, A., Cosma, A., Cheynier, R., Dereuddre-Bosquet, N., Le Grand, R., and Vaslin, B. (2014). Plasmacytoid dendritic cell dynamics tune interferon-alfa production in SIV-infected cynomolgus macaques. PLoS Pathog. *10*, e1003915.

Cheng, L., Ma, J., Li, J., Li, D., Li, G., Li, F., Zhang, Q., Yu, H., Yasui, F., Ye, C., et al. (2017). Blocking type I interferon signaling enhances T cell recovery and reduces HIV-1 reservoirs. J. Clin. Invest. *127*, 269–279.

Dave, V.P., Hajjar, F., Dieng, M.M., Haddad, É., and Cohen, E.A. (2013). Efficient BST2 antagonism by Vpu is critical for early HIV-1 dissemination in humanized mice. Retrovirology *10*, 128.

Donaghy, H., Pozniak, A., Gazzard, B., Qazi, N., Gilmour, J., Gotch, F., and Patterson, S. (2001). Loss of blood CD11c(+) myeloid and CD11c(-) plasmacytoid dendritic cells in patients with HIV-1 infection correlates with HIV-1 RNA virus load. Blood *98*, 2574–2576.

Folks, T.M., Clouse, K.A., Justement, J., Rabson, A., Duh, E., Kehrl, J.H., and Fauci, A.S. (1989). Tumor necrosis factor alpha induces expression of human immunodeficiency virus in a chronically infected T-cell clone. Proc. Natl. Acad. Sci. USA *86*, 2365–2368.

Harada, S., Koyanagi, Y., and Yamamoto, N. (1985). Infection of HTLV-III/LAV in HTLV-I-carrying cells MT-2 and MT-4 and application in a plaque assay. Science *229*, 563–566.

Harper, M.S., Guo, K., Gibbert, K., Lee, E.J., Dillon, S.M., Barrett, B.S., McCarter, M.D., Hasenkrug, K.J., Dittmer, U., Wilson, C.C., and Santiago, M.L. (2015). Interferon-α Subtypes in an Ex Vivo Model of Acute HIV-1 Infection: Expression, Potency and Effector Mechanisms. PLoS Pathog. *11*, e1005254.

Herbeuval, J.P., Grivel, J.C., Boasso, A., Hardy, A.W., Chougnet, C., Dolan, M.J., Yagita, H., Lifson, J.D., and Shearer, G.M. (2005a). CD4+ T-cell death induced by infectious and noninfectious HIV-1: role of type 1 interferon-dependent, TRAIL/DR5-mediated apoptosis. Blood *106*, 3524–3531.

Herbeuval, J.P., Hardy, A.W., Boasso, A., Anderson, S.A., Dolan, M.J., Dy, M., and Shearer, G.M. (2005b). Regulation of TNF-related apoptosis-inducing ligand on primary CD4+ T cells by HIV-1: role of type I IFN-producing plasmacytoid dendritic cells. Proc. Natl. Acad. Sci. USA *102*, 13974–13979.

Howell, D.N., Andreotti, P.E., Dawson, J.R., and Cresswell, P. (1985). Natural killing target antigens as inducers of interferon: studies with an immunoselected, natural killing-resistant human T lymphoblastoid cell line. J. Immunol. *134*, 971–976.

Huang, J., Yang, Y., Al-Mozaini, M., Burke, P.S., Beamon, J., Carrington, M.F., Seiss, K., Rychert, J., Rosenberg, E.S., Lichterfeld, M., and Yu, X.G. (2011). Dendritic cell dysfunction during primary HIV-1 infection. J. Infect. Dis. *204*, 1557–1562.

Ito, T., Kanzler, H., Duramad, O., Cao, W., and Liu, Y.J. (2006). Specialization, kinetics, and repertoire of type 1 interferon responses by human plasmacytoid predendritic cells. Blood *107*, 2423–2431.

Kwa, S., Kannanganat, S., Nigam, P., Siddiqui, M., Shetty, R.D., Armstrong, W., Ansari, A., Bosinger, S.E., Silvestri, G., and Amara, R.R. (2011). Plasmacytoid dendritic cells are recruited to the colorectum and contribute to immune activation during pathogenic SIV infection in rhesus macaques. Blood *118*, 2763–2773.

Lehmann, C., Jung, N., Förster, K., Koch, N., Leifeld, L., Fischer, J., Mauss, S., Drebber, U., Steffen, H.M., Romerio, F., et al. (2014). Longitudinal analysis of distribution and function of plasmacytoid dendritic cells in peripheral blood and gut mucosa of HIV infected patients. J. Infect. Dis. *209*, 940–949.

Lepelley, A., Louis, S., Sourisseau, M., Law, H.K., Pothlichet, J., Schilte, C., Chaperot, L., Plumas, J., Randall, R.E., Si-Tahar, M., et al. (2011). Innate sensing of HIV-infected cells. PLoS Pathog. *7*, e1001284.

Li, Q., Estes, J.D., Schlievert, P.M., Duan, L., Brosnahan, A.J., Southern, P.J., Reilly, C.S., Peterson, M.L., Schultz-Darken, N., Brunner, K.G., et al. (2009). Glycerol monolaurate prevents mucosal SIV transmission. Nature *458*, 1034–1038.

Li, H., Gillis, J., Johnson, R.P., and Reeves, R.K. (2013). Multi-functional plasmacytoid dendritic cells redistribute to gut tissues during simian immunodeficiency virus infection. Immunology *140*, 244–249.

Li, G., Cheng, M., Nunoya, J., Cheng, L., Guo, H., Yu, H., Liu, Y.J., Su, L., and Zhang, L. (2014). Plasmacytoid dendritic cells suppress HIV-1 replication but contribute to HIV-1 induced immunopathogenesis in humanized mice. PLoS Pathog. *10*, e1004291.

Li, G., Zhao, J., Cheng, L., Jiang, Q., Kan, S., Qin, E., Tu, B., Zhang, X., Zhang, L., Su, L., and Zhang, Z. (2017). HIV-1 infection depletes human CD34+CD38- hematopoietic progenitor cells via pDC-dependent mechanisms. PLoS Pathog. *13*, e1006505.

Lodge, R., Lalonde, J.P., Lemay, G., and Cohen, E.A. (1997). The membrane-proximal intracytoplasmic tyrosine residue of HIV-1 envelope glycoprotein is critical for basolateral targeting of viral budding in MDCK cells. EMBO J. *16*, 695–705.

Macal, M., Jo, Y., Dallari, S., Chang, A.Y., Dai, J., Swaminathan, S., Wehrens, E.J., Fitzgerald-Bocarsly, P., and Zuniga, E.I. (2018). Self-Renewal and Toll-like Receptor Signaling Sustain Exhausted Plasmacytoid Dendritic Cells during Chronic Viral Infection. Immunity *48*, 730–744.e5.

Marsden, M.D., and Zack, J.A. (2017). Humanized Mouse Models for Human Immunodeficiency Virus Infection. Annu. Rev. Virol. *4*, 393–412.

Masten, B.J., Olson, G.K., Kusewitt, D.F., and Lipscomb, M.F. (2004). Flt3 ligand preferentially increases the number of functionally active myeloid dendritic cells in the lungs of mice. J. Immunol. *172*, 4077–4083.

Melkus, M.W., Estes, J.D., Padgett-Thomas, A., Gatlin, J., Denton, P.W., Othieno, F.A., Wege, A.K., Haase, A.T., and Garcia, J.V. (2006). Humanized mice mount specific adaptive and innate immune responses to EBV and TSST-1. Nat. Med. *12*, 1316–1322.

Nganou-Makamdop, K., Billingsley, J.M., Yaffe, Z., O'Connor, G., Tharp, G.K., Ransier, A., Laboune, F., Matus-Nicodemos, R., Lerner, A., Gharu, L., et al. (2018). Type I IFN signaling blockade by a PASylated antagonist during chronic SIV infection suppresses specific inflammatory pathways but does not alter T cell activation or virus replication. PLoS Pathog. *14*, e1007246.

O'Brien, M., Manches, O., Sabado, R.L., Baranda, S.J., Wang, Y., Marie, I., Rolnitzky, L., Markowitz, M., Margolis, D.M., Levy, D., and Bhardwaj, N. (2011). Spatiotemporal trafficking of HIV in human plasmacytoid dendritic cells defines a persistently IFN-α-producing and partially matured phenotype. J. Clin. Invest. *121*, 1088–1101.

O'Brien, M., Manches, O., and Bhardwaj, N. (2013). Plasmacytoid dendritic cells in HIV infection. Adv. Exp. Med. Biol. *762*, 71–107.

Platt, E.J., Wehrly, K., Kuhmann, S.E., Chesebro, B., and Kabat, D. (1998). Effects of CCR5 and CD4 cell surface concentrations on infections by macrophagetropic isolates of human immunodeficiency virus type 1. J. Virol. *72*, 2855–2864.

Pulendran, B., Banchereau, J., Burkeholder, S., Kraus, E., Guinet, E., Chalouni, C., Caron, D., Maliszewski, C., Davoust, J., Fay, J., and Palucka, K. (2000). Flt3-ligand and granulocyte colony-stimulating factor mobilize distinct human dendritic cell subsets in vivo. J. Immunol. *165*, 566–572.

Reeves, R.K., Evans, T.I., Gillis, J., Wong, F.E., Kang, G., Li, Q., and Johnson, R.P. (2012). SIV infection induces accumulation of plasmacytoid dendritic cells in the gut mucosa. J. Infect. Dis. *206*, 1462–1468.

Sabado, R.L., O'Brien, M., Subedi, A., Qin, L., Hu, N., Taylor, E., Dibben, O., Stacey, A., Fellay, J., Shianna, K.V., et al. (2010). Evidence of dysregulation of dendritic cells in primary HIV infection. Blood *116*, 3839–3852.

Saïdi, H., Bras, M., Formaglio, P., Melki, M.T., Charbit, B., Herbeuval, J.P., and Gougeon, M.L. (2016). HMGB1 Is Involved in IFN-α Production and TRAIL Expression by HIV-1-Exposed Plasmacytoid Dendritic Cells: Impact of the Crosstalk with NK Cells. PLoS Pathog. *12*, e1005407.

Sandler, N.G., Bosinger, S.E., Estes, J.D., Zhu, R.T., Tharp, G.K., Boritz, E., Levin, D., Wijeyesinghe, S., Makamdop, K.N., del Prete, G.Q., et al. (2014). Type I interferon responses in rhesus macaques prevent SIV infection and slow disease progression. Nature *511*, 601–605.

Swiecki, M., and Colonna, M. (2015). The multifaceted biology of plasmacytoid dendritic cells. Nat. Rev. Immunol. *15*, 471–485.

Swiecki, M., Wang, Y., Vermi, W., Gilfillan, S., Schreiber, R.D., and Colonna, M. (2011). Type I interferon negatively controls plasmacytoid dendritic cell numbers in vivo. J. Exp. Med. *208*, 2367–2374.

Vanderford, T.H., Slichter, C., Rogers, K.A., Lawson, B.O., Obaede, R., Else, J., Villinger, F., Bosinger, S.E., and Silvestri, G. (2012). Treatment of SIV-infected sooty mangabeys with a type-I IFN agonist results in decreased virus replication without inducing hyperimmune activation. Blood *119*, 5750–5757.

Vandergeeten, C., Fromentin, R., Merlini, E., Lawani, M.B., DaFonseca, S., Bakeman, W., McNulty, A., Ramgopal, M., Michael, N., Kim, J.H., et al. (2014). Cross-clade ultrasensitive PCR-based assays to measure HIV persistence in large-cohort studies. J. Virol. *88*, 12385–12396.

Webster, B., Werneke, S.W., Zafirova, B., This, S., Coléon, S., Décembre, E., Paidassi, H., Bouvier, I., Joubert, P.E., Duffy, D., et al. (2018). Plasmacytoid dendritic cells control dengue and Chikungunya virus infections via IRF7-regulated interferon responses. eLife *7*, e34273.

Wimmers, F., Subedi, N., van Buuringen, N., Heister, D., Vivié, J., Beeren-Reinieren, I., Woestenenk, R., Dolstra, H., Piruska, A., Jacobs, J.F.M., et al. (2018). Single-cell analysis reveals that stochasticity and paracrine signaling control interferon-alpha production by plasmacytoid dendritic cells. Nat. Commun. *9*, 3317.

Zhang, Z., Cheng, L., Zhao, J., Li, G., Zhang, L., Chen, W., Nie, W., Reszka-Blanco, N.J., Wang, F.S., and Su, L. (2015). Plasmacytoid dendritic cells promote HIV-1-induced group 3 innate lymphoid cell depletion. J. Clin. Invest. *125*, 3692–3703.

Zhen, A., Rezek, V., Youn, C., Lam, B., Chang, N., Rick, J., Carrillo, M., Martin, H., Kasparian, S., Syed, P., et al. (2017). Targeting type I interferon-mediated activation restores immune function in chronic HIV infection. J. Clin. Invest. *127*, 260–268.

STAR★METHODS

KEY RESOURCES TABLE

REAGENT or RESOURCE	SOURCE	IDENTIFIER
Antibodies		
Mouse anti-human BDCA2	Liguo Zhang; Li et al., 2014	15B
Mouse anti-human BDCA2 (clone 201A)	BioLegend	Cat # 354214; RRID: AB_2563141
Mouse anti-human BDCA2 (clone 201A)	BioLegend	Cat # 354206; RRID: AB_11150412
Mouse anti-human CD2 (clone RPA-2.10)	BioLegend	Cat# 300232; RRID:AB_2800715
Mouse anti-human CD4 (clone OKT4)	BioLegend	Cat # 317428; RRID: AB_1186122
Mouse anti-human CD5 (clone UCHT2)	BioLegend	Cat# 300632; RRID:AB_2632671
Mouse anti-human CD8 (clone SK1)	BioLegend	Cat# 344730; RRID:AB_2564510
Mouse anti-human CD11c (clone 3.9)	BioLegend	Cat# 301633; RRID:AB_2561990
Mouse anti-human CD11c (clone 3.9)	BioLegend	Cat# 301635; RRID:AB_2562191
Mouse anti-human CD14 (clone M5E2)	BioLegend	Cat# 301822; RRID:AB_493747
Mouse anti-human CD16 (clone 3G8)	BioLegend	Cat# 302026; RRID:AB_2278418
Mouse anti-human CD19 (clone HIB19)	BioLegend	Cat# 302252; RRID:AB_2563560
Mouse anti-human CD45 (clone HI30)	BioLegend	Cat# 304014; RRID:AB_314402
Rat anti-mouse CD45 (clone 30-F11)	BioLegend	Cat# 103146; RRID:AB_2564003
Mouse anti-human CD56 (clone HCD56)	BioLegend	Cat# 318314; RRID:AB_604103
Mouse anti-human CD69 (clone FN50)	BioLegend	Cat# 310912; RRID:AB_314847
Mouse anti-human CD123 (clone 6H6)	BioLegend	Cat# 306024; RRID:AB_2562070
Mouse anti-human CD123 (clone 6H6)	BioLegend	Cat# 306017; RRID:AB_10900244
Mouse anti-human HLA DR (clone L243)	BioLegend	Cat# 307622; RRID:AB_493177
Mouse anti-human HLA DR (clone L243)	BioLegend	Cat# 307640; RRID:AB_2561913
Mouse anti-human IFNAR2 (clone MMHAR-2)	PBL Science	Cat # 21385-3; RRID: AB_605467
Mouse anti-human IFNAR2 (clone MMHAR-2)	PBL Science	Cat # 21385-9; RRID: AB_387828
Mouse anti-human IFNα (clone LT27:295)	Mitenyi Biotec	Cat # 130-099-214; RRID: AB_2659983
Mouse anti-human ILT7 (clone 17G10.2)	BioLegend	Cat# 326408; RRID:AB_2136375
Mouse anti-human Ki67 (clone B56)	BD Biosciences	Cat # 563757; RRID:AB_2688008
Mouse anti-HIV-1 core (clone KC57)	Beckmann Couter	Cat # 6604665; RRID:AB_1575987
Mouse anti-HIV-1 core (clone KC57)	Beckmann Couter	Cat # 6604667; RRID:AB_1575989
Mouse anti-human TNFα (clone MAb11)	BioLegend	Cat# 502909; RRID:AB_315261
Mouse isotype control IgG2a	BioXcell	Cat #: BE0085; RRID:AB_1107771
Bacterial and Virus Strains		
HIV: pCH077.t/2627	NIH AIDS Reagent Program	https://www.aidsreagent.org Cat # 11742
HIV: pNL4.3-ADA-GFP	Eric Cohen; Dave et al., 2013	N/A
Chemicals, Peptides, and Recombinant Proteins		
Brefeldin-A	Biolegend	Cat # 420601
Collagenase I	Sigma-Aldrich	Cat # C0130-1G
Collagenase V	Sigma-Aldrich	Cat # C9263-100MG
Collagenase XI	Sigma-Aldrich	Cat # C7657-1G
DNase (bovine pancrease)	Sigma-Aldrich	Cat # D4513-1VL
Hyaluronidase	Sigma-Aldrich	Cat # H3506-1G
Liberase (TL, Research grade)	Roche	Cat # 05401020001
Soluble Flt3L	Celldex Therapeutics	CDX-301
R848	InvivoGen	Cat # tlrl-r848
R848 (Vaccigrade)	InvivoGen	Cat # vac-r848

(*Continued on next page*)

Continued		
REAGENT or RESOURCE	SOURCE	IDENTIFIER
IFNα-2a	PBL Science	Cat # 11100-1
Critical Commercial Assays		
COBAS AmpliPrep/COBAS TaqMan HIV-1 test (Version 1)	Roche	https://diagnostics.roche.com/
Fixation/Permeabilization Solution Kit	BD Biosciences	Cat # 554714
Foxp3 transcription factor staining buffer set	eBioscience	Cat # 00-5523-00
Fixable violet dead cell stain kit	ThermoFisher	Cat # 34963
RNeasy Mini plus kit	QIAGEN Sciences	Cat # 74136
QIAamp DNA mini kit	QIAGEN Sciences	Cat # 51304
Human $CD34^+$ selection kit	Mitenyi Biotec	Cat # 130-100-453
Powerup Sybergreen Mastermix	Applied Biosystems	Cat # A25741
TaqMax Fast Advanced Master Mix	Applied Biosystems	Cat # 4444556
QIAzol Lysis Reagent	QIAGEN Sciences	Cat # 79306
Experimental Models: Cell Lines		
Human: ACH2 cells	NIH AIDS Reagent Program	NIH-ARP Cat# 349-443, RRID:CVCL_0138
Human: CEM.NKR-CCR5	NIH AIDS Reagent Program	NIH-ARP Cat# 4376-29; RRID:CVCL_X623
Human: HelaTZM bl	NIH AIDS Reagent Program	NIH-ARP Cat# 8129-442; RRID:CVCL_B478
Human: HEK-Blue IFN-α/β	InvivoGen	RRID:CVCL_KT26
Human: MT4	NIH AIDS Reagent Program	NIH-ARP Cat# 120-438, RRID:CVCL_2632
Human: 293T	ATCC	ATCC Cat# CRL-3216, RRID:CVCL_0063
Experimental Models: Organisms/Strains		
Mouse: NOD-*scid* IL2Rgamma^{null}	The Jackson Laboratory	https://www.jax.org/
Oligonucleotides		
Primer: GAPDH Forward: GCCATCAATGACCCCTTCATT	This paper	N/A
Primer: IFNα Forward: TCCATGAGVTGATBCAGCAGA	This paper	N/A
Primer: IRF7 Forward: GAGCCCTTACCTCCCCTGTTAT	This paper	N/A
Primer: Mx1 Forward: CAGCACCTGATGGCCTATCA	This paper	N/A
Primer: OAS1 Forward: TGTGTGTCCAAGGTGGTAAAG	This paper	N/A
Recombinant DNA		
psvCMV-VSV-G	Eric Cohen; Lodge et al., 1997	N/A
Software and Algorithms		
FACS Diva	BD Biosciences	https://www.bdbiosciences.com/en-us
FlowJo (Versions 9.9.3 and 10.1)	TreeStar	https://www.flowjo.com
Illustrator CC2018	Adobe	https://www.adobe.com
Prism (Versions 7 and 8)	GraphPad	https://www.graphpad.com

LEAD CONTACT AND MATERIALS AVAILABILITY

Further information and requests for reagents should be directed to and will be fulfilled by the Lead Contact, Eric A. Cohen (eric.cohen@ircm.qc.ca). This study did not generate new unique reagents. The plasmids psvCMV-VSV-G and HIV NL4.3-ADA-GFP are available from the Lead Contact with a completed Material Transfer Agreement so as to ensure adequate access to proper biosafety facilities.

EXPERIMENTAL MODEL AND SUBJECT DETAILS

Humanized NSG and BLT mice

NSG (NOD-*scid* IL2Rgamma^{null}) mice were acquired from the Jackson Laboratory. Cord blood-derived human CD34$^+$ hematopoietic stem cells (HSCs) were isolated by positive selection using human CD34$^+$ selection kit (Miltenyi Biotech). 10^5 of CD34$^+$ cells were injected i.v. into sublethally irradiated NSG mice (7 to 11 weeks old). Humanized bone marrow/liver/thymus (hBLT) mice were generated as previously described (Melkus et al., 2006). Briefly, human fetal thymus was implanted under the kidney capsula of 6 to 10-week old NSG mice. In addition to the thymic implant, mice also received (i.v.) autologous fetal liver CD34$^+$ HSCs ($5x10^5$). Prior to humanization, all mice were preconditioned using gamma radiation with 1 to 2 Gy. Efficiency of humanization was monitored by flow cytometry analysis of human immune cell subsets. Characteristics of humanized mice used in this study can be found in Table S1. The Table also provided information pertinent to the gender of mice used in different experiments. Given the nature of the experimental system used (i.e., humanized mice), mouse gender per se did not have any bearing on the results. Typically, humanized NSG mice were used when they were about 17 to 19 weeks post humanization whereas BLT mice were usually used when they were about 8-10 weeks post humanization.

Human cord blood and autologous fetal thymus and liver were obtained from the Cord Blood Research Bank, Sainte-Justine Hospital following written informed consent from donors and approval of a research protocol by the Centre Hospitalier Universitaire (CHU) Sainte-Justine institutional review board (CER#2126). Fetal tissues were obtained from a local abortion clinic through our clinical collaborator (J.V.G) and the donors provided written consent prior to acquisition of tissues. As per the Ethic's guidelines, no information regarding the donors were provided to us. Mice were maintained in specific pathogen-free animal facility of CHU Sainte-Justine Research Center or in the animal core facility of the Montreal Clinical Research Institute in accordance with protocols approved by each institution's Institutional Animal Care and Use Committee (IRCM 2015-11 and CIBPAR#582&593). All experiments performed were approved and conformed to the regulatory standards set by the Committees.

Cell lines

HEK293T cells (ATCC) were generated from epithelial cells that were originally isolated from a female fetal kidney tissue. The HeLa TZM-bl cell line (Platt et al., 1998), acquired from the NIH AIDS reagent program, was generated from HeLa cells, a cell line derived from a 30-year-old female patient with papillomavirus-related endocervical adenocarcinoma. HEK-Blue IFN-α/β reporter cells, obtained from InvivoGen, were generated from the parental HEK293 cell line as aforementioned. HEK293T, HeLa TZM-bl and HEK-Blue cells were grown in DMEM media (10% FBS supplemented with Penicillin-streptomycin). The T cell lines CEM.NKR-CCR5 (Howell et al., 1985), MT4 (Harada et al., 1985) and ACH-2 (Folks et al., 1989) were obtained from the NIH AIDS reagent program. CEM.NKR-CCR5 cells were derived from the parental CEM T cell line and the latter was isolated originally from a 4-year-old female patient with lymphoblastic leukemia. MT4 cells were obtained by co-culture of leukemic cells from a male patient with male cord blood lymphocytes. ACH-2 cells were generated from a CEM T cell line subclone and contained one copy of the integrated proviral HIV-1. All three CD4$^+$T cell lines were maintained in RPMI 1640 media supplemented with 10% FBS and Penicillin-streptomycin. All cultured cells were maintained at 37°C and 5% CO_2.

Measurements of bioactive IFN-I using HEK-Blue IFN-α/β reporter cells

Bioactive IFN-I was quantified in plasma using HEK-Blue IFN-α/β reporter cells (InvivoGen) according to manufacturer's instructions. Three-fold serial dilutions of recombinant IFN-α (PBL Science) were used as quantitative standards. IFN-I levels were extrapolated from the linear range of the standard curve generated from the quantitative standards mentioned above.

Primary cell cultures: *ex vivo* stimulation of splenocytes with HIV-infected CD4$^+$ T cells and TLR7/8 agonist Resiquimod R848

MT4 cells were infected with VSV-G pseudotyped, CCR5-tropic NL4.3-ADA-GFP for 48h and at the time of co-culture with splenocytes, approximately 15%–30% were GFP$^+$. Splenocytes (10^6 in 500 μl), seeded in a 24-well plate were co-cultured with infected MT4 cells (120,000) for 12h. Alternatively, 10^6 splenocytes (200 μl in a 96-well U-bottom plate) were treated with R848 (10 μg/mL; Invivogen) for 3h. Following the stimulation, Brefeldin-A (BioLegend) was added and cells were cultured for another 6h. Splenocytes that did not receive the agonist or those cultured with mock-infected MT4 cells were used as negative controls. Subsequently, cells were stained for cell surface markers of interest followed by intracellular staining for IFN-α and TNF-α as described below.

METHOD DETAILS

Virus production

$5x10^6$ HEK293T cells (obtained from ATCC) were transfected with 20 μg of CCR5-tropic pNL4.3-ADA-GFP proviral DNA (Dave et al., 2013), or pCH077.t/2627 (NIH AIDS reagent program) by the calcium phosphate method. To prepare the virus used in co-culture assays, HEK293T cells were co-transfected with pNL4.3-ADA-GFP and pCMV-VSV-G (Lodge et al., 1997). Culture supernatant was

collected at 60 h post-transfection. Virus was concentrated by ultracentrifugation over a 20% sucrose cushion and titered in HeLa TZMbl and CEM.NKR-CCR5 cells (both lines were from the NIH AIDS reagent program). $TCID_{50}$ was calculated using the Spearman-Karber method.

Flt3L treatment, infection of humanized mice and quantification of viral loads

Flt3L (CDX-301) was kindly provided by Celldex Therapeutics (Hampton, NJ). H-NSG and hBLT were treated daily with Flt3L (2 μg, i.p.) for 11 days before infection and every two days thereafter. This dose was equivalent to 75 μg/kg, previously found to be non-toxic and well tolerated in human studies (Anandasabapathy et al., 2015).

Humanized NSG and BLT mice were infected (i.p.) with 500,000 and 200,000 $TCID_{50}$ of virus in 100 μl of DMEM, respectively. Uninfected mice were injected with 100 μl of sterile DMEM medium. Plasma HIV-1 viral loads were determined using the quantitative COBAS AmpliPrep/COBAS TaqMan HIV-1 test, version 2.0, Roche (detection limit, < 20 copies/ml).

Depletion of human pDC and blocking of type I IFN (IFN-I) signaling

To deplete pDC *in vivo*, 15B, a mAb specific to blood dendritic cell antigen-2 (BDCA-2) was used (Li et al., 2014). In brief, hNSG were treated (i.p) with 15B (100 μg, equivalent to 4 mg/kg) on alternate day for 5 days before infection and every two days thereafter. Control mice were injected with isotype control IgG2a (Bioxcell).

To block IFN-I signaling, mice were injected with anti-IFNAR2 mAb (clone MMHAR2, PBL Science) (i.p., 100 μg) 24h before infection and every 2 days thereafter (Zhen et al., 2017). Control mice were injected with isotype control IgG2a. To confirm blocking of the pathway, hNSG mice previously treated with Flt3L for 11 days were injected with 100 μg of the anti-IFNAR2 Ab (or isotype control) for 6 h followed by a 13-hour stimulation with the TLR7/8 agonist Resiquimod R848 (Vaccigrade, InvivoGen) (Cheng et al., 2017). Analysis of ISGs was performed in spleen cells by real-time PCR. In certain cases, efficiency of binding of the anti-IFNAR2 mAb to the receptor *in vivo* was assessed by flow cytometry using PE-conjugated anti-IFNAR2 mAb (clone MMHAR2, PBL Science).

Cell isolation from peripheral blood and tissues

Mice were bled at different time points before and after infection. Plasma was collected and white blood cells were isolated by treating whole blood with red blood cell lysis buffer (Invitrogen).

Infected mice were sacrificed by gas anesthesia overdose and intra-cardiac puncture. Cardiac perfusion was performed before tissues were harvested. BM cells were isolated from the femur using the needle method. To purify splenocytes, spleens were crushed and passed through a 40-μm cell strainer (BD Biosciences) to yield single-cell suspensions. Lung and liver tissues were digested with a mixture of enzymes (all from Sigma-Aldrich) containing collagenase I (135 U), collagenase XI (27.5 U), hyaluronidase (18 U) and DNase (18 U) in 2 mL of HBSS (Wisent) for 1 h at 37°C. Cell suspensions were filtered through a sterile 70-μm cell strainer and cells purified by centrifugation over 40% and 80% Percoll gradients (Sigma). Cells from GALT were prepared as follows. In brief, intestines were cut into 1-cm pieces and bathed with gentle agitation (450 rpm) in RPMI supplemented with 10% FBS, 5 mM EDTA and 0.145 mg/ml of DTT for 20 min at 37°C. The tissue was further digested in RPMI containing 750 μg of Liberase, 2 mg of Collagenase V and 173 μg of DNase for 1 h at 37°C with agitation (500 rpm). Single-cell suspension was obtained by passing the sample through 100-μm and subsequently, 70-μm cell strainers.

Flow cytometry

Blood cells and single-cell suspensions from tissues were stained with fluorescently labeled Abs as desired. Dead cells were excluded using live/dead fixable violet dead cell stain kit (ThermoFisher). Surface-stained cells were fixed and permeabilized using the Cytofix/Cytoperm kit (BD Biosciences) as per manufacturer's instructions and intracellularly stained for HIV-1 p24 or for IFN-α and TNF-α. Flow cytometry data were collected on a Fortessa flow cytometer (BD Bioscience) and analyzed by Flowjo software (Versions 9.9.3 and 10.1).

Nucleic acid extraction and quantification of HIV genomes and human genes by real-time PCR

RNA from splenocytes or other tissues were extracted using RNeasy Mini plus kit or QIAzol Lysis Reagent (both were from QIAGEN) according to manufacturer's instructions. cDNA was generated using Superscript II reverse transcriptase (Invitrogen) and used as templates for HIV RNA analysis or cellular genes as detailed below. Total DNA from tissue-derived cells were extracted using QIAamp DNA mini kit (QIAGEN) according to manufacturer's instructions. Total and integrated HIV DNA were quantified by modified nested real-time PCR assay using Taq DNA polymerase (BioLabs) in the first PCR and TaqMax Fast Advanced Master Mix (Applied Biosystems) in the second PCR (Vandergeeten et al., 2014). DNA from serially diluted ACH-2 cells (NIH AIDS Reagent Program) was extracted and amplified in parallel to generate a standard curve from which unknown samples were enumerated. Human CD3 gene was used as a normalizer. Cellular gene mRNA was quantified using Powerup Sybergreen Mastermix (Applied Biosystems) and primers: GAPDH 5′- GCCATCAATGACCCCTTCATT (forward) 5′- TTGACGGTGCCATGGAATTT (reverse); IFN-A 5′-TCCAT GAGVTGATBCAGCAGA (forward) 5′-ATTTCTGCTCTGACAACCTCCC (reverse); IRF7 5′-GAGCCCTTACCTCCCCTGTTAT (forward) 5′-CCACTGCAGCCCCTCATAG (reverse); Mx1 5′- CAGCACCTGATGGCCTATCA (forward) 5′- ACGTCTGGAGCATGAAGAACTG (reverse); OAS1 5′- TGTGTGTCCAAGGTGGTAAAG (forward) 5′- TGAGAGGACTGAGGAAGACAA (reverse).

QUANTIFICATION AND STATISTICAL ANALYSIS

Data analysis was performed using GraphPad Prism (Version 7). Descriptive measures (mean, median, minimum/maximum range and percent) were used to summarize the data. Non-parametric Mann-Whitney's U-tests (two-tailed) were used to compare ranks between two treatment groups. Two-tailed Wilcoxon matched-pairs rank test to compare expression level of HLA DR and CD40 before and after TLR7 stimulation. Pearson correlation analysis was performed to determine if there was an association between plasma IFN-I levels and viral loads. Linear regression was performed prior to Pearson analysis to assess if the relationship between the variables was linear. A *P value* of less than 0.05 was considered statistically significant. *, **, ***, **** signify < 0.05, < 0.01, < 0.001, < 0.0001, respectively; ns, not significant. No statistical methods were used to predetermine population size. Randomization was not used.

DATA AND CODE AVAILABILITY

This study did not generate any unique datasets or code.